Noname manuscript No.
(will be inserted by the editor)

Investigating spatially developing turbulent boundary layers with uniform blowing using a one-dimensional stochastic turbulence model

Rakhi · D. O. Lignell · H. Schmidt

Received: date / Accepted: date

Abstract A spatially evolving turbulent boundary layer with uniform blowing is investigated using a map-based stochastic One-Dimensional Turbulence (ODT) model. An understanding of turbulent fluxes with blowing for the reduction of skin friction is of significant importance for mitigating the environmental impact, especially for reducing the fuel consumption in major transportation systems. The ODT model is computationally efficient due to the reduction in dimensionality and the flow variables are resolved on a full range of time and length scales. These variables are evolved by a deterministic process representing the molecular diffusion and a stochastic process modelling the effect of turbulent advection and pressure fluctuation. The reduced dimensionality makes ODT particularly appropriate for high Reynolds number flow. In this paper, we compare the results obtained from ODT to recent Large Eddy Simulations (LES) data at moderate momentum thickness Reynolds numbers up to $Re_\theta = 2500$, based on the free-stream velocity and the momentum-loss thickness. The amplitude of uniform blowing is set as 0.1% of the free-stream velocity to investigate the effect on the skin friction drag. The comparison is presented for $Re_\theta \approx 1407, 2082$, and 2395 for a fixed free-stream velocity and blowing magnitude. The ODT model is capable of reproducing several velocity statistics, such as the mean velocity and the turbulent stresses compared to available reference data. ODT can also capture various trends observed as a result of blowing, for example, enhanced Reynolds stresses and reduction of skin friction. The results presented in this paper corroborate that ODT is

Rakhi (✉) · H. Schmidt
Department of Mechanical Engineering, Electrical and Energy Systems, BTU Cottbus-Senftenberg, Cottbus, Germany
E-mail: rakhi.rakhi@b-tu.de

D. O. Lignell
Department of Chemical Engineering, Brigham Young University, Provo, UT 84602, USA

an economical and reasonably accurate approach to investigate the effect of blowing on the skin friction drag.

Keywords One-Dimensional Turbulence · stochastic modeling · turbulent boundary layers · drag reduction · boundary layer control

1 Introduction

To control turbulent wall-bounded flows, the mechanism of adding or removing the mass through a porous surface has led to extensive studies of such kind of problems over the last decades. In case of adding the mass, i.e., blowing, the skin friction drag is reduced, while removing the mass by suction results in drag enhancement [1–3]. The fluid viscosity on the surface of vehicles causes the skin friction drag, which drastically increases by the turbulent transition of the flow and has a large economical and ecological impact from a fuel consumption point of view. For reducing the fuel consumption in major transportation systems (for example, aircraft, trains and ships), the reduction of skin friction drag in turbulent flows is of great importance. Apart from this, the drag reduction for aerial vehicles have positive ramifications such as a larger operational range, greater endurance and higher achievable speeds.

A variety of ideas have been devised for the skin friction drag reduction and to control other flow properties. Numerous passive [4,5] and active [6,7] flow control techniques have been used. A majority of studies, however, focus on internal flows. Due to practical importance, external flows are investigated via blowing and suction. The spatially developing turbulent boundary layer (SBL) with blowing or suction from a spanwise localized slot have been performed in [8] by DNS and in [9] by means of LES. The drag reduction effects of blowing generated by a microblowing plate have been reported in [10]. An identity equation decomposing the skin friction drag into a laminar component and a turbulent component for the canonical internal flows was introduced in [11] which was later used in several studies related to the external flows. In addition to that, a DNS of the SBL with uniform blowing and suction was performed in [2] and experimentally in [10,12]. However, the DNS [2] was performed at a low Reynolds number, $Re_\theta = 300$. Recently, the effect of uniform blowing and suction with a finite streamwise length of the uniform blowing/suction region has been studied in [3] up to $Re_\theta = 2500$.

Nevertheless, further investigations are still required for the effective and practical drag reduction in external flows. Additionally, a large computational domain is required due to inhomogeneity in the streamwise and wall-normal directions in the SBL canonical flow [13–17]. Particularly in the case of DNS, to gather the complete information of the flow, very high spatial resolution is required and hence, limited to small and moderate momentum Reynolds numbers [18], i.e., $Re_\theta = 4300$ for SBL without blowing [15] and $Re_\theta = 300$ with blowing [2]. However, the Reynolds number is much higher in engineering applications [19,20]. To achieve moderate Reynolds numbers, LES have been performed in [21] for $Re_\theta = 8300$ in case of SBL without blowing and in [3]

for blowing/suction up to $Re_\theta = 2500$. In the case of LES as well as RANS, the spatio-temporal development of the flow cannot be very well captured as compared to DNS.

To resolve small scale flow variables and to achieve high Reynolds number, a lower-order formulation is crucial. In the formulation presented here, the Navier-Stokes equations are modelled on a 1-D computational domain. In this formulation, the flow variables are resolved by a deterministic process which represents molecular diffusion terms [22,23]. The effect of nonlinear advection and fluctuating pressure gradient terms are modelled by a stochastic process. The reduced-order formulation, i.e., one-dimensional turbulence (ODT) achieves major cost reductions compared to DNS/LES through reduced spatial dimensionality, hence, making high Reynolds number simulation feasible.

In the present paper, we utilize stand-alone ODT to investigate the effect of uniform blowing in a turbulent boundary layer. We do not expect to capture all aspects of a full 3-D DNS or LES with a reduced order model. The main focus is to check predictability of the model and the flow physics captured by introducing uniform blowing in the cross-stream direction. More complex flows can be investigated by embedding the ODT lines in a coarse 3-D LES mesh referred as ODTLES [24–26].

The paper is organized as follows: Section 2 presents a brief overview of the ODT model with the required formulation for the present case. The ODT simulation set-up is provided in Section 3. The optimal model parameter selection to capture the flow dynamics is given in Section 4. Section 5 addresses the predictive capabilities of ODT for the velocity statistics and various global properties. These results are compared to the available reference LES data from [3] up to $Re_\theta = 2500$. Finally, Section 6 presents the major conclusions of our analysis.

2 ODT: One-Dimensional Turbulence

The main features of the ODT model are summarized in this section. Starting with an overview of the model, we present the governing equations, the formulation of the eddy events, the selection of these events and some important physical model parameters of ODT.

2.1 Overview of the model

Before moving to the formulation of the model, we first present a brief overview summarizing the applications of ODT.

A major advantage of ODT is to permit economical simulations of high Reynolds number turbulence over the full range of dynamically relevant length scales allowing physically sound representation of interactions between turbulent advection and microphysical processes [23]. The demonstration of a degree of commonality among turbulent flow phenomena (which might not

otherwise be readily apparent) by capturing diverse flow behaviors within a concise modeling framework based on broadly applicable empirical principles [22,23] is another benefit of the model. The lack of an unique, kinematically and dynamically consistent analogy between the 1-D model formulation and the 3-D turbulent flow under consideration is, however, an inherent limitation of the ODT model [22].

The first formulation of ODT was given in [22] which was later extended by including pressure scrambling effects [23]. Gradually the model was extended and applied to a variety of flows. The applications of the model includes channel [27,28], pipe [29], multi-physics and reactive flows [30–37] and other complex cases [24,25,36,38,26,29] among others. Relating to boundary layers, a limited validation of a case involving forcing of a boundary layer flow is discussed in [28]. Stably-stratified boundary layers are presented in [39]. An asymptotic suction boundary layer displaying a temporal evolution running to a statistical steady state is investigated in [40]. The flow dynamics captured for the temporally developing turbulent boundary layer is reported in [41–43] using temporal ODT. The study was further extended in [44,45] using spatial ODT.

In this paper, ODT is applied to investigate the effects of uniform blowing in SBL for the first time. A good reason for validating the ODT spatial formulation with blowing is because it is practically useful and effective in order to achieve high Reynolds numbers relevant for engineering applications. However, the main aim of the present paper is only to check predictability of the model by introducing uniform blowing and check the behaviour of the turbulent statistics and global properties with the considered flow configuration.

2.2 Governing equations

In the ODT model, a stochastic implementation of 1-D eddy events is coupled to the deterministic solution of a 1-D diffusion evolution equation. The effects of turbulent transport due to eddies on the 1-D property profiles of the flow are modelled by instantaneous eddy events and the deterministic diffusion process occurs between these events. We describe the deterministic diffusion equations followed by the eddy event implementation.

The governing equations in ODT can be expressed in a temporal formulation (T-ODT) as well as a spatial formulation (S-ODT). We explain both formulation of the model below, but for the present study only the spatial formulation of the model is utilized. We follow the Lagrangian framework described in [28], where the planar form of the governing equations are derived in detail. For a detailed derivation of the ODT equations in Lagrangian and Eulerian forms, we refer to [46]. The ODT domain is aligned with the wall-normal direction y in both approaches. The expression for streamwise momentum equation for T-ODT in the planar case [28] is described as,

$$\frac{\partial u}{\partial t} + EE = \nu \frac{\partial^2 u}{\partial y^2}. \tag{1}$$

The first term of the equation represents the local change of the velocity vector with respect to time t. The second term EE, the stochastic eddy events term, represents the effect of the turbulent advection and fluctuating pressure gradient forces due to the turbulent eddy motions. This term couples the velocity component depending on the instantaneous flow state of $u(y,t)$ and will be explained later. The right hand side of Eq. (1) represents the viscous forces involving the kinematic viscosity ν. The continuity equation for uniform properties inside the control volume in 1-D is trivially conserved in the Lagrangian formulation, where cell faces are allow to move such that the mass in a cell is constant.

The incompressible condition is trivially satisfied in case of the stochastic eddy event component because the triplet map is measure preserving. In the deterministic evolution of the diffusive advancement equations, the incompressible condition is satisfied since, for a 1-D model, the mean advecting velocity along the line is zero. The term EE is zero in between the implementation of two subsequent eddy events, hence the 1-D diffusion equations need to be integrated from one instantaneous eddy event to the next. For the numerical solution, the diffusion part of Eq. (1) is discretized by a first-order explicit Euler method with a grid-adaptive finite-volume method.

Equation (1) for S-ODT, as used for the present investigation, can be expressed as [28],

$$u\frac{\partial u}{\partial x} + v\frac{\partial u}{\partial y} + EE = \nu\frac{\partial^2 u}{\partial y^2}. \tag{2}$$

The local changes of the velocity vector with respect to the longitudinal direction x is represented by the first term of the above equation. This formulation allows simulation of flows that are statistically 2-D [28], but steady in time (not considering the stochastic eddy events). The spatial formulation conserves the $y-$mass flux instead of conserving the mass in a cell.

2.3 Formulation of the eddy events

The term EE in Eqs. (1) and (2) represents the eddy events. These events occur through the instantaneous displacement of the fluid elements to represent a turbulent stirring motion. This process modifies any property profile over the ODT line interval $[y_0, y_0 + l]$, with y_0 as the lower edge of a notional eddy and l its size. The eddy events are implemented by using the triplet map. The triplet map induces fluid displacement and fulfills two other fundamental requirements. First, that the mapping is measure preserving, and second, it does not introduce spatial discontinuities.

The triplet map essentially takes a property profile in an eddy region and replaces it with three copies of the original. Each copy is spatially compressed by a factor of three and the middle copy is spatially inverted in order to avoid discontinuities. This correlates with a physical mapping, that is, an advective transport of fluid from a given location $f(y)$ to a new location y. The mapping

function $f(y)$ is given as [22]

$$f(y) = y_0 + \begin{cases} 3(y-y_0), & y_0 \le y \le y_0 + l/3 \\ 2l - 3(y-y_0), & y_0 + l/3 \le y \le y_0 + 2l/3 \\ 3(y-y_0) - 2l, & y_0 + 2l/3 \le y \le y_0 + l \\ (y-y_0), & \text{otherwise.} \end{cases} \tag{3}$$

To represent the effects of fluctuating pressure gradient that cause return-to-isotropy effects, the mapped velocity field, $\mathbf{u}\big(f(y),t\big)$ (or $\mathbf{u}\big(f(y),x\big)$ for S-ODT) is modified to allow energy redistribution among velocity components with the aid of a kernel function and a coefficient vector $\mathbf{c} = (c_1, c_2, c_3)^{\mathrm{T}}$ [23] as

$$EE : \begin{cases} \mathbf{u}(y,t) \to \mathbf{u}\big(f(y),t\big) + \mathbf{c}\,K(y) & \text{T-ODT,} \\ \mathbf{u}(y,x) \to \mathbf{u}\big(f(y),x\big) + \mathbf{c}\,K(y) & \text{S-ODT.} \end{cases} \tag{4}$$

Note that there is no uniquely preferable form of the kernel function $K(y)$. However, it is convenient to relate it to the fluid displacement induced by the mapping $f(y)$, that is, $K(y) = y - f(y)$ [22]. An important physical constraint is satisfied by this choice which makes the kernel function nonzero only in the eddy interval $[y_0, y_0 + l]$. $K(y)$ integrates to zero which ensures that there are no artificial momentum sources regardless of the selection of the components c_i, where $i \in \{1, 2, 3\}$. Some caution, however, has to be taken in the selection of c_i to ensure that the kinetic energy is not artificially generated but only redistributed among the velocity components.

To determine the coefficients c_i, the change of the kinetic energy ΔE_i in the ith velocity component due to the application of Eq. (4) is considered [23] and this change of the kinetic energy is given as (ρ is the density)

$$\Delta E_i = \begin{cases} \dfrac{\rho}{2} \displaystyle\int_{y_0}^{y_0+l} \Big(\Big[u_i\big(f(y),t\big) + c_i\,K(y) \Big]^2 - u_i^2(y,t) \Big)\, \mathrm{d}y & \text{T-ODT,} \\ \dfrac{\rho}{2} \displaystyle\int_{y_0}^{y_0+l} \Big(\Big[u_i\big(f(y),x\big) + c_i\,K(y) \Big]^2 - u_i^2(y,x) \Big)\, \mathrm{d}y & \text{S-ODT.} \end{cases} \tag{5}$$

Energy is conserved when the sum of the individual contributions ΔE_i vanishes, i.e., $\Delta E_1 + \Delta E_2 + \Delta E_3 = 0$. This constrains the selection of c_i because each velocity component has a finite amount of energy that can be added to or removed from the other two components.

To find an appropriate energy scale, the extractable kinetic energies ($-\Delta E_i$) are maximized with respect to the c_i. This yields the maximum extractable energy, Q_i, for component i as

$$Q_i = \frac{1}{2\hat{K}} \rho l u_{i,K}^2, \tag{6}$$

where the two kernel-weighted quantities $u_{i,K}$ and $\hat{K}$ are

$$u_{i,K} = \begin{cases} \dfrac{1}{l^2}\displaystyle\int_{y_0}^{y_0+l} u_i\big(f(y),t\big)\,K(y)\,\mathrm{d}y & \text{T-ODT}, \\ \dfrac{1}{l^2}\displaystyle\int_{y_0}^{y_0+l} u_i\big(f(y),x\big)\,K(y)\,\mathrm{d}y & \text{S-ODT}, \end{cases} \tag{7}$$

and

$$\hat{K} = \frac{1}{l^3}\int_{y_0}^{y_0+l} K^2(y)\,\mathrm{d}y. \tag{8}$$

A model parameter α is introduced that controls the fraction of each of the extractable (available) kinetic energies that is actually redistributed:

$$\Delta E_i = -\alpha Q_i + \frac{\alpha}{2}Q_j + \frac{\alpha}{2}Q_k. \tag{9}$$

Here, (i,j,k) represents cyclic permutations of (1,2,3). The model parameter α varies in the range $[0,1]$. $\alpha = 0$ means there is no transfer of the kinetic energy, $\alpha = 2/3$ means equipartition of the energies, and $\alpha = 1$ represents maximal transfer of the kinetic energy. That α is not fixed reflects that the pressure fluctuations do not necessarily imply a maximization of the inter-component kinetic energy transfers. Equations (6) and (9) are inserted in Eq. (5) to obtain the coefficients c_i encountered in Eq. (4):

$$c_i = \frac{1}{\hat{K}l}\left(-u_{i,K} + \mathrm{sgn}(u_{i,K})\sqrt{(1-\alpha)u_{i,K}^2 + \frac{\alpha}{2}u_{j,K}^2 + \frac{\alpha}{2}u_{k,K}^2}\right), \tag{10}$$

where sgn represents the sign function.

2.4 Eddy event selection

For the above formulated eddy events, it is essential to determine the location y_0, size l, and time of occurrence t (or streamwise position of occurrence x for S-ODT). These stochastic variables are governed by an 'eddy rate distribution' $\lambda(y_0,l,t)$ or $\lambda(y_0,l,x)$ [22]. Here $\lambda(y_0,l,t)\,\mathrm{d}y_0\,\mathrm{d}l\,\mathrm{d}t$ specifies the number of eddies in the size range $[l, l+\mathrm{d}l]$, position range $[y_0, y_0+\mathrm{d}y_0]$ and during a time interval $[t, t+\mathrm{d}t]$. Note that for S-ODT, the time interval is replaced by a space interval $[x, x+\mathrm{d}x]$. The form for λ is given by

$$\lambda(l,y_0,t) = \frac{C}{l^2\,\tau(l,y_0,t)}. \tag{11}$$

In this equation, τ represents the eddy turnover time which depends on the instantaneous flow state. C is a model parameter and scales the overall rate of the eddy events in the flow. This parameter needs to be estimated for a given flow configuration as the turbulence intensity in general depends on the prescribed forcing mechanism. Constructing λ isn't hard, sampling the eddy PDF, which is defined in terms of λ is difficult. The actual implementation

constructs λ directly for each eddy event, but we don't know whether those eddy events make sense because we don't construct the actual eddy PDF. The eddy PDF is λ/Λ, where Λ is the total rate of all eddies. But to get that would require evaluating λ for all sizes and locations, and that is expensive to do considering that it changes as soon as an eddy event or diffusive advancement occurs.

The spatial analogue of the eddy rate distribution, λ can be written as [22, 47, 29]

$$\lambda(l, y_0, x) = \frac{C\tilde{v}_\epsilon}{l^2\,\xi(l, y_0, x)}. \tag{12}$$

Here, ξ is the eddy streamwise increment related to the instantaneous flow state and $\tilde{v}_\epsilon$ is the Favre averaged velocity in the eddy region.

Now, to calculate τ in Eq. (11), the specific kinetic energy l^2/τ^2 contained in the eddy motion is considered in T-ODT, whereas for S-ODT it becomes $l^2\tilde{v}_\epsilon^2/\xi^2$. This energy should be similar to the extractable kinetic energy given in Eqs. (5) and (6), maintaining consistency of the formulation. This yields

$$\frac{l^2}{\tau^2} \sim \sum_{i=1}^{3} u_{i,K}^2 - Z\frac{\nu^2}{l^2}, \tag{13}$$

$$\frac{l^2\tilde{v}_\epsilon^2}{\xi^2} \sim \sum_{i=1}^{3} u_{i,K}^2 - Z\frac{\nu^2}{l^2}, \tag{14}$$

for T-ODT and S-ODT, respectively. Summation of $u_{i,K}^2$ in the above equations (instead of ΔE_i) indicates the fact that the total extractable kinetic energy does not depend on the model parameter α, i.e., the inter-component energy transfer. The last term on right hand side of Eqs. (13) and (14) represents the damping effects of the viscosity, and Z is a model parameter which allows suppression of small eddies.

Once the location y_0 and size l of an eddy event have been selected, the eddy time scale τ for T-ODT and eddy streamwise increment ξ for S-ODT, respectively, is computed from the instantaneous velocity profiles $u_i(y,t)$ or $u_i(y,x)$ as

$$\frac{1}{\tau} = \sqrt{\frac{1}{l^2}\sum_{i=1}^{3} u_{i,K}^2 - Z\frac{\nu^2}{l^4}}, \tag{15}$$

$$\frac{1}{\xi} = \frac{1}{\tilde{v}_\epsilon}\sqrt{\frac{1}{l^2}\sum_{i=1}^{3} u_{i,K}^2 - Z\frac{\nu^2}{l^4}}. \tag{16}$$

The eddy time scale τ and the mean sampling time scale τ_s are compared to obtain the acceptance probability $p_a = (\tau/\tau_s)^{-1} < 1$ ($(= \xi/\xi_s)^{-1} < 1$ for S-ODT) of a physically plausible eddy event. For this purpose, τ (ξ) needs to be computed at a specific instant (or x location) that is sampled as a marked Poisson process. The eddy events are assumed to be independent of each other

in this process, such that the time (streamwise increment) between two such events can be sampled economically from an exponential distribution. But the rejection process introduces a dependence as the eddy acceptance depends on the property profiles that are affected by the previous eddy events. For more detail, we refer the reader to [22].

It is sometimes important to suppress the unphysically large eddy events which may occur seldomly in the sampling procedure. For this purpose, a large-eddy suppression (LS) is often used. A simple suppression based on the fraction of the domain length [28,29] may be sufficient for confined flows, like channel or pipe flows. The elapsed-time method [31,30] is preferred for free shear flows, such as jets, in which only eddy events satisfying $\tau \leq \beta_{LS}\, t$ are allowed, ($l \leq \beta_{LS}\, x$ for S-ODT) where t is the current simulation time and β_{LS} a model parameter [31]. Here, β_{LS} is used as 0.8 which is taken from TBL case [41]. For boundary layer type flows, the shear can be highly concentrated in a thin layer close to the wall. Although the associated shear in an eddy is nearly zero in almost all parts of its size range, an unphysical large eddy event could still be accepted, this could be avoided by using the two-thirds LS mechanism [47]. In this mechanism, the eddy interval is subdivided into three equidistant subsections with the purpose of verifying that the eddy is energetically feasible in at least two of these subsections.

3 Simulation set-up

For the present ODT simulations, we have used the similar simulation set-up which is used for LES in [3]. The schematic for ODT simulation set-up is shown in Figure 1. The SBL is realized on the computational domain of the ODT model by prescribing no-slip conditions at the bottom wall and Neumann conditions at the open domain with $u = u_\infty$, $\frac{\partial v}{\partial y} = \frac{\partial w}{\partial y} = 0$. The streamwise velocity component u has been initialized with a laminar profile and the other two velocity components (v, w) are initialized to zero.

Blowing is achieved by the constant wall-normal velocity on the bottom wall, v_0. This is shown in Figure 1. To establish blowing, a Lagrangian method is used in which the mesh is evolved by marching the ODT domain away from the wall [28,36]. No extra source term is required for this case. The amplitude of uniform blowing is set to be 0.1% of the free-stream velocity, i.e, $v_0 = 1.0 \times 10^{-3}\,\mathrm{m/s}$. We have utilized a dynamic C++ adaptive code to carry out the simulations [28]. The important numerical parameters associated with the mesh adaptions are the minimum and maximum allowed grid size (dx_{min}, dx_{max}) enabled during the adaption. dx_{min} and dx_{max} must be spaced sufficiently from each other for the dynamic mesh adaption procedure. For the present study, these values are used from the reference paper [3]. The physical model parameters used to carry out the simulations are summarized in Table 1.

The data is gathered until the statistical convergence of the desired quantities is achieved and this is done on an ensemble basis using at least N=1000 members representing individual ODT realizations. These members are run

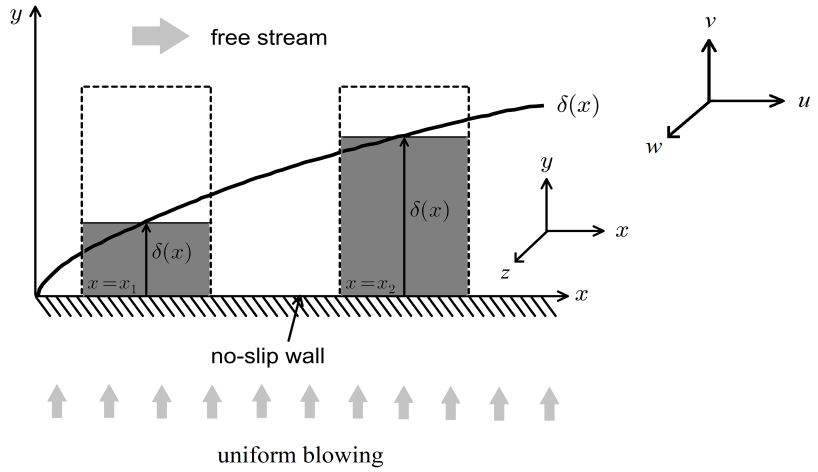

Fig. 1 A schematics of the spatially developing turbulent boundary layer (SBL) with uniform blowing.

in parallel on a large computing cluster and are autonomous so that communication is not a limiting factor. For this, the seed of the underlying random generator is varied while using the same initial conditions.

Other numerical parameters are the maximum (L_{max}), minimum (L_{min}) and most probable (L_p) eddy size. It is unnecessary to sample very large eddy events as the boundary layer thickness must remain sufficiently smaller than the domain size. Such eddy events are unphysical and instantly rejected by the large eddy suppression mechanism. The L_{max} corresponds to 60% of the domain size to increase the performance of the model. L_{min} is estimated as the Kolmogorov length scale, η, with the aid of pre-simulations. L_p is taken as three times of the minimum eddy size to capture the initial transient stage. Apart from these numerical parameters, the important physical model parameters, α, C and Z as well as the large eddy suppression (LS), have been described in Section 2.

The simulations are carried out for momentum thickness Reynolds number, $Re_\theta = \theta u_\infty/\nu$ up to 2500, where θ is the momentum layer thickness, ν is the kinematic viscosity of the fluid and u_∞ is the free stream velocity. ν is fixed as $1.5 \times 10^{-5}\,\mathrm{m}^2/\mathrm{s}$ (air). We have compared the velocity statistics with the reference data for $Re_\theta \approx 1407, 2082$, and 2395.

We define the friction, thickness, and displacement Reynolds numbers for future reference as,

$$Re_\tau = \frac{u_\tau\,\delta_{99}}{\nu}, \quad Re_{\delta_{99}} = \frac{u_\infty\,\delta_{99}}{\nu}, \quad Re_X = \frac{u_\infty\,x}{\nu}. \tag{17}$$

Table 1 Summary of the cases and model parameters. These are the physical model parameters.

Case	C	Z	α	LS
U1C1	3	100	2/3	two-thirds
U1C2	9	100	2/3	two-thirds
U1Z1	6	1	2/3	two-thirds
U1Z2	6	300	2/3	two-thirds
U1L1	6	100	2/3	elapsed time
U1L2	6	100	2/3	frac. domain
U1	6	100	2/3	two-thirds

In the first equation u_τ is the frictional velocity. The thickness δ_{99} in the first and the second equation serves as the outer length scale of the solution. In the last equation, x is the streamwise length scale.

Note that the usual convention is followed to investigate effects of blowing and the variables are rescaled to the inner units, i.e., viscous units denoted with the superscript '+'. For example, $u^+ = u/u_\tau$ and $y^+ = y/y_\tau$, where u_τ is the frictional velocity calculated as $u_\tau = \sqrt{\tau_0/\rho}$ with $\tau_0 \equiv -\mu\partial\overline{u}/\partial y\,|_0 > 0$ and y_τ is the viscous length scale, i.e., $y_\tau = \nu/u_\tau$. Some of the figures use '$-$' as superscript which represents the outer unit scaling using u_∞ and δ_{99}.

4 Model parameter assignment

The sensitivity of the results to the physical ODT model parameters (α, C, Z, and the large-eddy suppression) are discussed below. The ODT results are compared to the reference LES [3] at $Re_\theta \approx 2082$ to find the optimal set of model parameters for the blowing configuration. Previous studies have shown that these parameters are not universal and are generally configuration-specific. For example, wall-bounded flows [22,24,39], mixing layers [47], thermal convection [48], and non-reacting and reacting jets [31,30,29], require different ODT model parameters. The pipe and jet flow are treated with the same set of parameters in [29] and in a third reactive jet case, C is increased to get reasonable results compared to experiments. These studies demonstrate that the selection of the model parameters is influenced by the physics included and the forcing mechanism used in the flow and hence need to be tuned for a given flow configuration.

To find the optimal set of parameters, we start with the set of model parameters for the asymptotic suction boundary layer [40] and TBL [41] because these studies are close to our present work. The transfer coefficient parameter α, controls the exchange of the turbulent energy between the three velocity components. The value for this parameter can vary from zero to one and $\alpha = 2/3$ means equipartition of energy in the velocity components. In most of the previous studies α is 2/3 and we use the same value for the blowing configuration. The other parameters C, Z, and the large-eddy suppression

are calibrated against the reference LES case [3]. Note that while calibrating one particular parameter, all other parameters are kept fixed. We found that the range of these parameters, in comparison with the earlier studies [41], is very small and the ODT simulations are carried out for $C \in \{3, 6, 9\}$, $Z \in \{1, 100, 300\}$ and 'two-thirds', 'elapsed time' and 'frac domain' mechanism for large eddy suppression.

We have considered the mean velocity profile for selecting the model parameters by comparing to the LES results [3]. Note that the mean velocity profile obeys the same near-wall similarity solution for all ODT solutions discussed in this section and only the friction velocities u_τ are different.

4.1 Variation of the model parameter C

The C parameter is referred to as the turbulent intensity parameter. This parameter controls the frequency of the eddy events or the overall turbulence of the flow. The flow is laminar for the small C values because fewer eddies are implemented for small values of C. The opposite behavior is observed for large values of C.

The influence of the C parameter on the mean streamwise velocity scaled with the inner units, u_τ and y_τ and with the outer units u_∞ and δ_{99} is depicted in Figure 2(a) and (b), respectively. The use of the inner units are indicated by the superscripts '+' and the outer units by '−'. The reference LES data [3] is not available in the outer units and is shown only in the inner units.

Figure 2(a) displays the impact of the C parameter on the slope of the normalized velocity profile in the logarithmic region and also on the frictional velocity, u_τ. The flow dynamics remain unaltered in the inner region, i.e., $y^+ < 20$ and the slope is changed in the logarithmic region, i.e., $y^+ > 30$. Spread in the curve at high y values is due to the inner scaling, u_τ. Fewer eddies are implemented for the small C values which reduces the level of turbulence of the flow. For large C values, we note opposite behaviour with increased turbulence intensity and hence u_τ. We achieve a good match for the mean velocity between the ODT results and the reference LES data [3] for $C = 6$ and this value is used to carry out the ODT simulations. The boundary layer flow is most sensitive to the C parameter [41,44].

To see how much the shape change in Figure 2(a) is explained by the faster boundary layer growth for larger C, the mean velocity profile is scaled in the outer units. Figure 2(b) shows that a fairly good large-y collapse is obtained and the profiles collapse very well for all C values considered in the range $y^- = y/\delta_{99} > 0.1$ suggesting that the large-scale dynamics as well as the growth of the outer layer are comparable in the two respective cases. The streamwise mean velocity is $u^-_\infty = 1$. Note that the outer units are most sensitive to the C parameter.

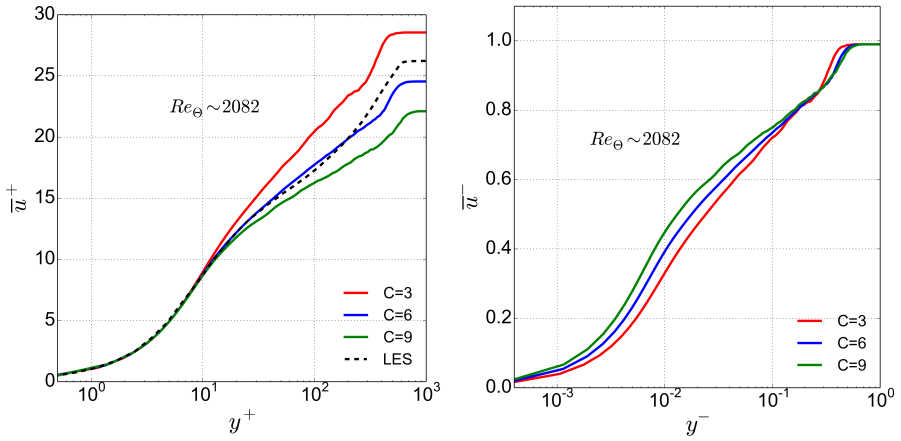

(a) (b)

Fig. 2 Normalized wall-normal profiles of the (a) mean streamwise velocity $\overline{u}$ for various values of the model parameter C at $Re_\theta \approx 2082$. ODT results are shown in comparison to a reference LES [3] at corresponding Re_θ. The model parameters $\alpha = 2/3$, $Z = 100$ and the large-eddy suppression are fixed. (b) Same data as in (a) but normalized with the outer velocity, u_∞, and length scale, δ_{99}. The superscripts '+' and '−' indicate normalization with inner and outer units, respectively.

4.2 Variation of the model parameter Z

The model parameter Z is utilized to suppress the eddy events that are smaller than the Kolmogorov scale by using $Z > 1$. This mechanism increases the efficiency of the algorithm in the model. In the buffer layer, for the wall bounded flows, the 3-D eddies behave different in comparison to the 1-D representation in the ODT model. Since the Z parameter affects the starting point of the buffer layer, a good match is obtained between the ODT solutions and the LES [3] data by excluding eddies larger than the Kolmogorov ones by selecting $Z > 1$ [24]. The ODT simulations are carried out for $Z \in \{1, 100, 300\}$ for the mean velocity profile at $Re_\theta \approx 2082$ in comparison with the LES data [3] at the same Re_θ. While performing the sensitive analyses for Z parameter, the other parameters are kept fixed.

Figure 3(a) and (b) depicts the impact of the Z parameter on the mean streamwise velocity profile scaled with the inner and the outer units, respectively. The representation of both the units remains same as explained in previous section for the C parameter.

Figure 3(a) shows that the Z parameter is less sensitive to the mean velocity profile than the C parameter for uniform blowing case. Nevertheless, a well know effect of the Z parameter is confirmed and we note an upward shift of the mean velocity profile in the logarithmic region with increasing Z. This upward shift of $\overline{u}^+$ is due to the decrease of u_τ. However, the effect is small

suggesting that the Z parameter controls the mean shear across the viscous sublayer and has negligible effect on the logarithmic region of the turbulent boundary layer with uniform blowing.

Figure 3(b) show a better horizontal alignment of the profiles because the Z parameter has less effect than the C parameter on the occurrence of large eddies that control the boundary layer growth. For the blowing case, we choose $Z = 100$ for further investigation. Note that the value of the Z parameter considered for the uniform blowing configuration is smaller as compared to the other ODT applications [28,29,40,41]. This indicates that the small eddies are important in case of blowing and are included to capture the flow properties.

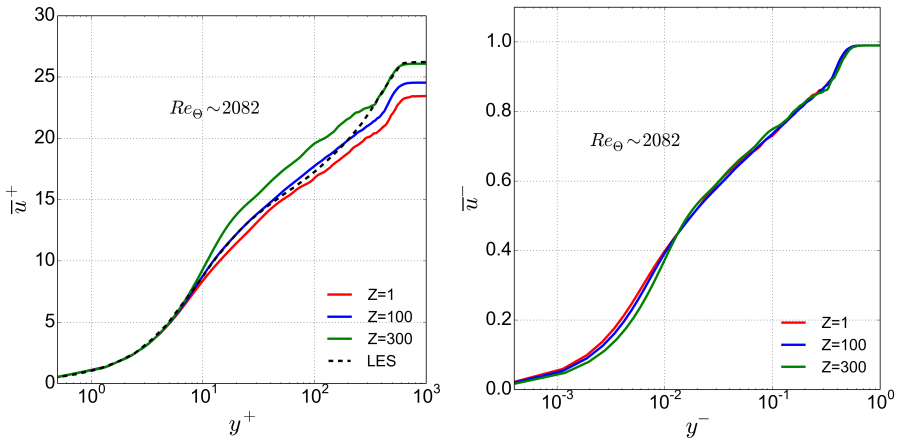

Fig. 3 Same as Figure 2 but for the variation of the model parameter Z.

4.3 Influence of the large-eddy suppression mechanism

The large eddy suppression (LS) is an important feature introduced to avoid a large-scale anomaly. The occasional occurrence of large eddy events may dominate the total transport as their turnover time is more than the current run time of the simulations and hence these eddies should be avoided. There are different ways implemented in the model [28,29,31,30,47,22] to restrict such large eddies explained in Section 2. These eddies can be restricted by 'frac domain', 'elapsed time', or 'two-thirds' LS mechanisms. The influence of these suppression mechanisms on the mean velocity profile is checked for $Re_\theta \approx 2082$ in comparison to the reference LES data [3] at the same Re_θ.

The influence of the LS mechanism on the mean streamwise velocity component scaled with the inner and the outer units are presented in Figure 4(a)

and (b), respectively. The representation of both the units remains same as explained in previous sections for the C and Z parameters. While performing the simulations with LS, all the other parameters are fixed at their optimal values.

In the viscous sublayer, there is no influence of the LS mechanism on the mean velocity profile as shown in Figure 4(a) and hence the near-wall similarity solution is obeyed for all ODT solutions. As the large eddy events affect mainly the outer layer, the influence is observed in the region $y^+ > 10$ and the velocity profile agrees with the LES data for the two-thirds LS mechanism. On the other hand, for the other two suppression mechanisms, the profiles are not only under-predicted but also do not reproduce qualitative behaviour of the two-thirds mechanism and the LES data. For the elapsed time mechanism, the profile in the buffer region as well as outer log region, is same as for the frac domain mechanism. The LS suppression mechanisms impact the outer region the most and, as a result, u_τ, as well as the normalized free-stream velocity $\overline{u}^+$ is altered.

Figure 4(b) shows the mean streamwise velocity profile in the outer units and explains the shape change by the faster boundary layer growth for the LS mechanism. We note a good large-y collapse for the elapsed time and frac domain mechanism. The LS mechanism has more effect than the Z parameter on the occurrence of large eddies that control the boundary layer growth. For the blowing case, we choose the two-thirds mechanism for further investigation.

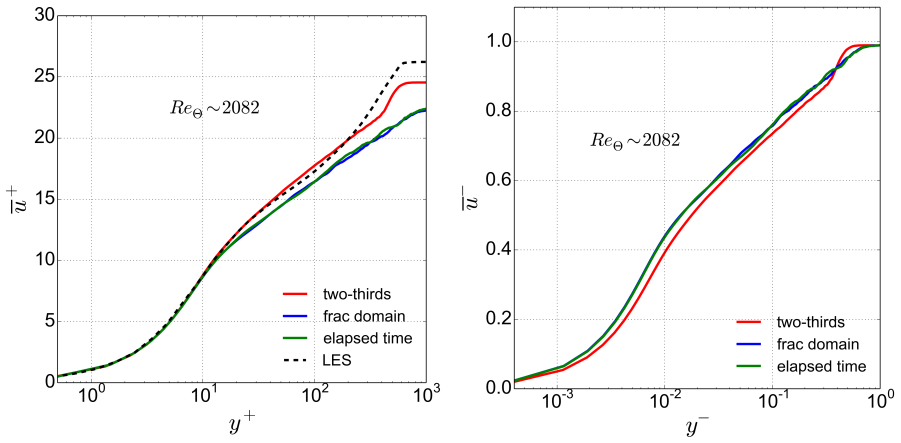

(a) (b)

Fig. 4 Same as Figure 2 but for the various large-eddy suppression (LS) methods.

5 Results

In this section, we have discussed the velocity statistics up to 4^{th} order at some selected streamwise locations for $Re_\theta \approx 1407, 2082$ and 2395 in comparison to the available reference LES data from [3] at the same Re_θ. Note that not all the statistics are available for the uniform blowing flow configuration. So, for comparison purposes, we have used some of the DNS profiles from the non-blowing SBL configuration from [15]. Later in the section, some of the structural properties, for example, Re_τ, H and C_f as a function of Re_θ are also discussed. The simulations are performed for one free-stream velocity with the optimal set of the physical model parameters fixed at $\alpha = 2/3$, $C = 6$, $Z = 100$, and the two-thirds large-eddy suppression mechanism.

5.1 First and second order velocity statistics

The mean streamwise velocity profiles as a function of the wall-normal coordinate in viscous units for (a) $Re_\theta \approx 1407, 2082$ and 2395 for uniform blowing case and (b) $Re_\theta \approx 1811$ and 2047 for non-blowing case, for a fixed free-stream velocity along with the LES reference [3] (dashed lines) is depicted in Figure 5. The ODT profiles shows very good agreement with the reference LES data at given Re_θ for the selected optimal parameters. The velocity profile is independent of Re_θ from the inner region to the buffer region up to $y^+ < 200$. Conversely, in the outer region, the velocity profile for the low Re_θ case is somewhat nearer the wall than the other two higher Re_θ cases. This trend is consistent for the ODT and the LES, but the effect is slightly stronger for the ODT. This demonstrate the ability of the ODT model to capture the variations for the mean velocity from the inner region to the buffer region and further into the log-region for the spatially developing turbulent boundary layer with uniform blowing.

The pre-multiplied mean velocity gradient, i.e., the indicator function is shown in Figure 6 for $Re_\theta \approx 1407, 2082$ and 2395. The indicator function calculated as $y^+ \left(\partial \overline{u}^+ / \partial y^+\right)$ is plotted as a function of the wall-normal coordinate in viscous units for uniform blowing. Note that we do not have LES data for comparison and we have used the DNS data of a fully turbulent zero pressure gradient SBL from [18] plotted as a black dashed line at $Re_\theta \sim 2000$.

The indicator function is important because it aids in assessing if there is a logarithmic region in the mean velocity profile. The log-region is identified in the velocity profile by a constant region in the plot. The profiles are independent of Re_θ from the inner to the buffer region and dispersed in the region far away from the wall.

We now consider the von Kármán constant K of the law of the wall in order to address the similarity properties. K is determined as the inverse of the pre-multiplied mean velocity gradient, i.e., indicator function in the logarithmic region. While there is no clear logarithmic region for the case considered, K is obtained by averaging indicator function over $25 \leq y^+ \leq 150$

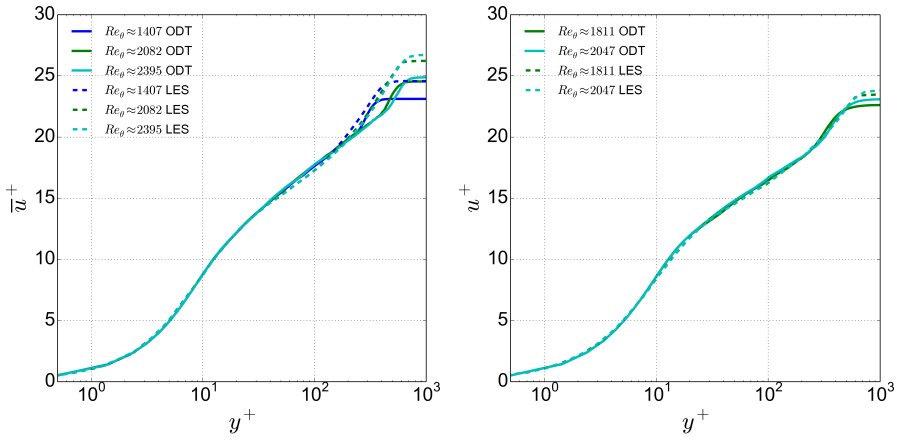

(a) (b)

Fig. 5 The mean streamwise velocity profile as a function of the wall-normal coordinate (in viscous units) (a) for uniform blowing case at $Re_\theta \approx 1407, 2082$ and 2395 and (b) non-blowing case at $Re_\theta \approx 1811$ and 2047. For comparison, the reference LES data for uniform blowing and non-blowing configurations from [3] at corresponding Re_θ are shown.

(given in Table 2 for $Re_\theta \approx 2395$). $K = 0.32$ for the spatially developing turbulent boundary layer with uniform blowing. The ODT model captures the qualitative trends from the reference DNS data using the estimated set of physical model parameters.

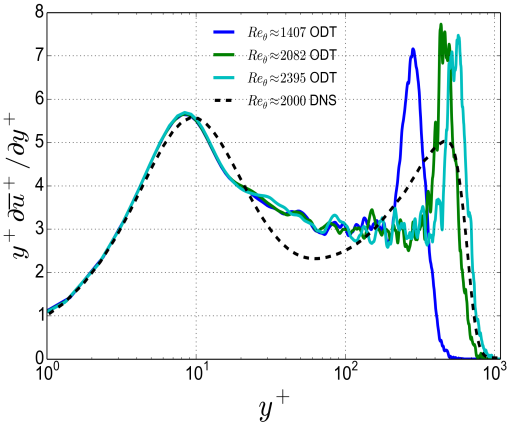

Fig. 6 The indicator function versus wall-normal coordinate (in viscous units) at $Re_\theta \approx 1407, 2082$ and 2395. For comparison, the reference DNS data for the SBL configuration from [18] at $Re_\theta \sim 2000$ is given by a black dashed line.

Figure 7(a) displays the root mean square (rms) of the streamwise velocity component ($u^+_{rms} = \sqrt{\overline{u'^2}}/u_\tau$) as a function of the normalized wall-normal coordinate in viscous units. The profiles are shown for three Re_θ, i.e., $Re_\theta \approx 1407, 2082$ and 2395 in comparison with the reference LES data from [3] at corresponding Re_θ. We know from previous studies [22,23,28,40,41] that the ODT model under-predicts the rms peaks due to the missing 3-D information. Therefore, we need to retain some 3-D information [24,35] to get a good fit for the rms profiles using ODT in comparison to the reference LES [3]. The peak value for the rms profile can be improved by choosing a small value of the model parameter C.

The general trend for rms is similar to the reference LES [3] with increasing Re_θ. The rms profiles remain unaffected by changes in Re_θ in the inner region up to $y^+ < 10$ and show sensitivity to Re_θ from $y^+ > 10$ onward. The peak amplitude is directly proportional to the Re_θ. An additional peak in the outer log-region was reported in [44] at small Re_θ and in [41] at all Re_θ. This peak was attributed purely to the transient flow, or to the effect of the initial conditions in [44], and also to the LS method used and the time window selected in [41]. For the present uniform blowing case we also use the same LS method as used in [41] but we do not use any time window since we are using streamwise position to calculate Re_θ instead of temporal points. This peak is also discerned in the DNS results for high bulk Reynolds number [49] and it has decreased after the initial transient has passed leaving a 'shoulder'. This 'shoulder' appears in the reference LES data as well [3]. Therefore, ODT seems to capture this general property of the outer layer dynamics of the boundary layer.

When compared with the TBL and SBL non-blowing cases [41,44] and for the present case considered shown in Figure 7(b), we note a slight increase in the rms amplitude by blowing. This is due the reduced skin friction coefficient which will be discussed shortly.

Figure 7(c) shows the profiles for the normalized cross stresses as a function of the wall-normal coordinate in viscous units, ($\overline{u'v'}/u_\tau^2$), for all three Re_θ. The reference data from [3] is plotted with dashed lines for corresponding Re_θ. Note that the calculation of the cross stresses is different in ODT and is based on the changes of the velocity profiles due to eddies (see [22] Appendix C). An additional peak was reported in temporal and spatial boundary layer investigation in [41,44] for non-blowing cases and this peak is also discerned in Figure 7(d), which we do not capture for the uniform blowing configuration (Figure 7(c)). This indicates that the flow dynamics may be different for the different flow configuration.

The qualitative trend for the cross stress profiles show agreement with the LES data [3]. However, the profiles are under-predicted as compared to the reference data. Interestingly, the cross stresses for the suction boundary layer [40] were reported to be over-predicted compared to DNS data. For the temporally developing turbulent boundary layer, the cross stresses were in very good agreement with the DNS results and it was slightly under-predicted

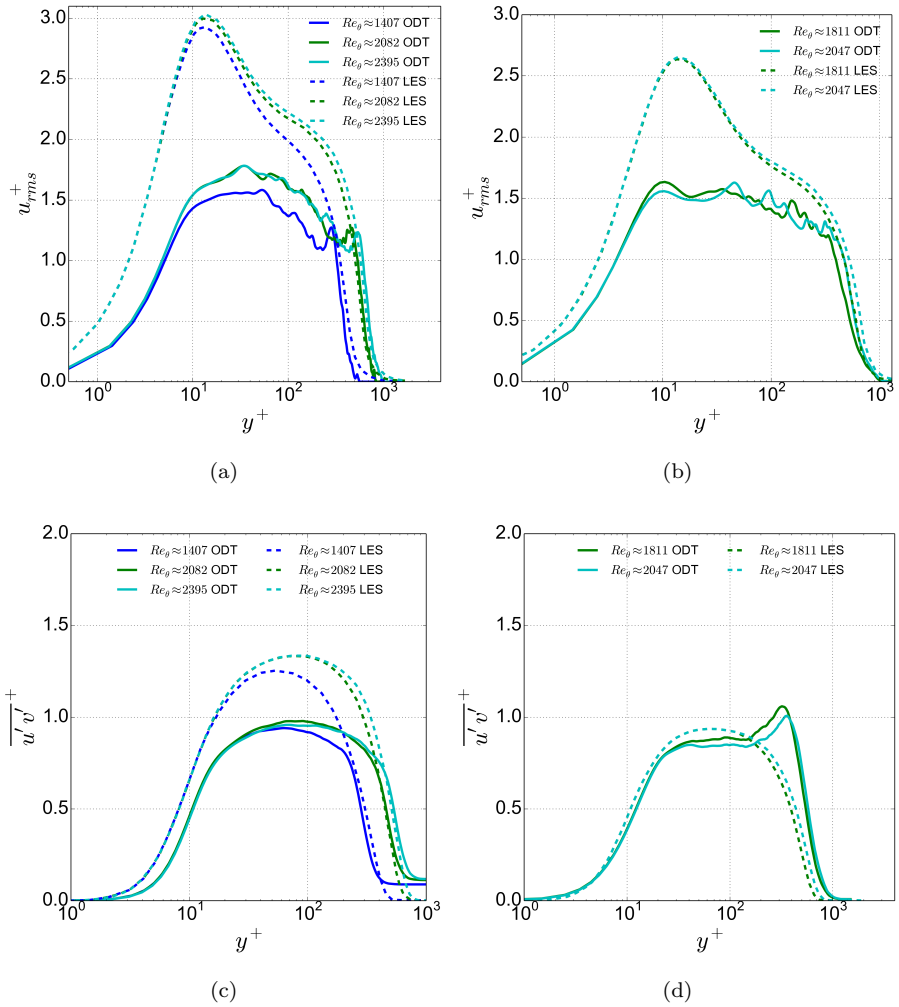

Fig. 7 (a) Streamwise root-mean-square velocity profiles and (c) profiles of the cross stresses, for uniform blowing case at $Re_\theta \approx 1407, 2082$ and 2395. (b,d) Same data as in (a,c) but for non-blowing case at $Re_\theta \approx 1811$ and 2047. All quantities are functions of the wall-normal coordinate in viscous units. For comparison, the reference LES data from [3] at corresponding Re_θ is shown for uniform blowing and non-blowing configuration.

for the spatially developing turbulent boundary layer. This lends confidence in the predictive capabilities of ODT for the selected flow configuration.

5.2 Higher order velocity statistics

The turbulent production as a function of the wall-normal coordinate in viscous units is depicted in Figure 8. The turbulent production is calculated as $-\overline{u'v'}^+ \frac{\partial \overline{u}^+}{\partial y^+}$. The figure displays production for the same Re_θ values as discussed above for the other velocity statistics. Note that we do not have production data for the reference LES for selected Re_θ. A modest comparison is made by using the DNS data for non-blowing case from [15] at comparable Re_θ, i.e., $Re_\theta \approx 2000$. As expected in case of uniform blowing, we note the peak of production is slightly over-predicted for the ODT simulations in comparison to the DNS data. This might be due to the reduction in skin friction coefficient for present configuration. Nevertheless, the qualitative trend remains unaltered for the blowing configuration and we do not observe dependence of production on Re_θ. Note that the cross stress profiles shown in Figure 7(c) are under-predicted, but the production curve is very close to the reference data, suggesting the $\partial u/\partial y$ is over-predicted (see Figure 6).

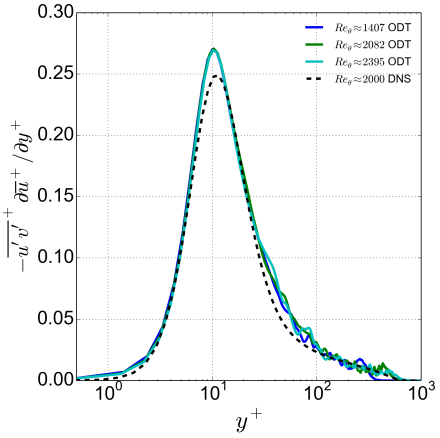

Fig. 8 The turbulent kinetic energy production as a function of the wall-normal coordinate (in viscous units) at $Re_\theta \approx 1407, 2082$ and 2395 for uniform blowing configuration. For comparison, the reference DNS data from [15] at $Re_\theta \approx 2000$ is shown for the non-blowing SBL configuration.

Figure 9(a) depicts the skewness of the streamwise velocity component, $-\overline{u'^3}/u_{rms}^3$, as a function of the wall-normal coordinate in viscous units, y^+. Note that we do not have the reference LES data for the blowing configuration for higher order velocity statistics and, similar to the production, we show the DNS data from [15] at $Re_\theta \approx 2000$, whereas for ODT, the profiles are displayed at three Re_θ as discussed above for the first and second order velocity statistics. The skewness behaves similar to the non-blowing spatial and temporal simulations reported in [41,44] in the inner region, i.e., $y^+ < 10$.

Some deviations are discerned in the buffer region, $10 < y^+ < 100$, for the blowing configuration in comparison to the non-blowing spatial boundary layer [44]. Nevertheless, the skewness profiles are consistent with the temporal simulations performed using T-ODT [41]. The behaviour for the skewness was different in the case of a suction boundary layer [40]. The ODT results are qualitatively consistent with the DNS data considered. The dependence of the skewness on Re_θ is dominant in the outer log-region, i.e., $y^+ > 300$. For more details regarding the skewness produced using the ODT model, we refer the reader to our earlier work [41,44], where we have briefly discussed the skewness features and deviations from the reference data.

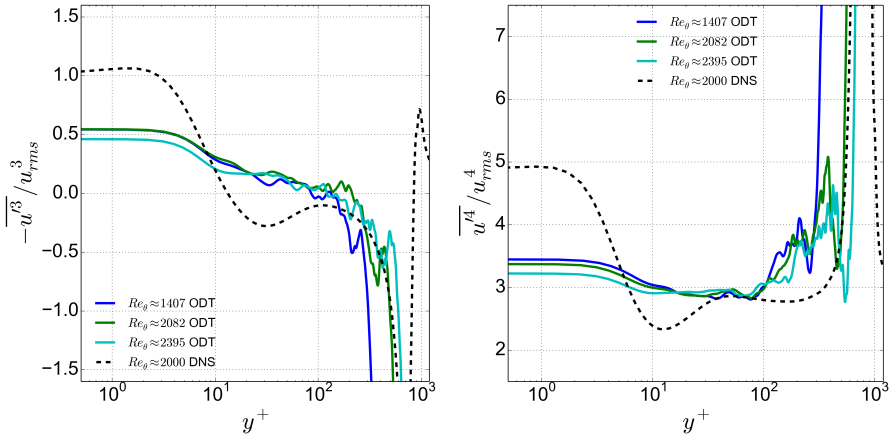

(a) (b)

Fig. 9 Profiles of the (a) skewness and (b) flatness of the streamwise velocity fluctuations as a function of the wall-normal coordinate in viscous units at $Re_\theta \approx 1407, 2082$ and 2395 for uniform blowing configuration. For comparison, the reference DNS data from [15] at $Re_\theta \approx 2000$ is shown for the non-blowing SBL configuration.

Next, we show the flatness of the streamwise velocity component, $\overline{u'^4}/u_{rms}^4$, as a function of the wall-normal coordinate in viscous units depicted in Figure 9(b) for the uniform blowing case at $Re_\theta \approx 1407, 2082$ and 2395. For comparison, we show the DNS data from [15] at $Re_\theta \approx 2000$ in dotted lines for SBL. The flatness profiles are under-predicted in the inner region, i.e., $y^+ < 10$, near the wall and over-predicted in the buffer region, $10 < y^+ < 40$ in comparison to the reference data. While the agreement of the ODT flatness profile with DNS doesn't look good, it is worth to note that this is a high order statistic, which will cause small differences in the flow to be amplified in this statistic. The fourth order velocity statistics show reasonable agreement with the DNS data along a certain y range from moderate to large distance from the wall. Like the mean velocity profiles and the rms profiles, flatness also

show dependency on Re_θ in the outer log-region. The outer layer statistics in ODT are dominated by the kernel-mechanism explained in [41,44].

In general, ODT is more Gaussian than DNS and the Gaussian flatness value for the ODT model is 3, which is same as reported in [41]. ODT might be more Gaussian than DNS because DNS is more dynamic. Giving some more context, we note that the ensemble is built by the ODT simulation runs with identical initial conditions but different random number sequences. These are realized by initializing with different random seeds. On average, all ensemble members develop in time in a similar way but all of them are uncorrelated when looking at the flow profiles at a particular point in time. This property manifests itself — not surprisingly at all — by virtually perfect Gaussianity of the point statistics. This would be different in DNS, for example, when a similar ensemble of the flow profiles would be constructed from the spanwise direction as these profiles would be spatially correlated (provided they are reasonably close to each other). However, this is not the case for the present ODT application.

We attribute the flatness disagreement with the reference DNS data to the missing 3-D information. Hence, we might need to retain some 3-D information of the flow to reproduce the 4^{th} order velocity statistics. A non-standalone application of ODT, referred to as ODTLES [25] can be used to overcome the above limitation and it permits the simulations of much more complex flows by largely removing the one-dimensional constraint.

5.3 Variation of the global properties with Re_θ

In this section, we have presented some of the global properties as a function of Re_θ. We have shown below the frictional Reynolds number (Re_τ), shape factor (H), and skin friction coefficient (C_f) with Re_θ up to $Re_\theta \approx 2500$ for uniform blowing configuration and up to $Re_\theta \approx 3000$ for the non-blowing case. The respective cases considered are represented as 'B-' for blowing and 'NC-' for no control in the figures discussed in this section for a fixed free-stream velocity. For comparison, the reference LES data from [3] is plotted with a dashed line for all the global properties. Table 2 summarises the values of the properties achieved at the last sampled Re_θ.

Figure 10 displays the variation of Re_τ with Re_θ to further quantify the turbulence in the near-wall region. The spatial development of Re_τ is calculated using u_τ and δ_{99} (see Table 2). The figure also shows a functional relation for the two Reynolds numbers, i.e., Re_τ in terms of Re_θ where we note a linear behaviour of the quantities. For the blowing configuration, a power-law relation is obtained as $Re_\tau = 0.61 \times {Re_\theta}^{0.92}$ to provide a good fit for the ODT data. The given equation can be used to convert between Re_τ and Re_θ. We also report this relation for non-blowing configuration as $Re_\tau = 0.76 \times {Re_\theta}^{0.89}$ and note that the value reached for Re_τ at any Re_θ is less in the case of uniform blowing in comparison to a non-blowing case. A decrease of Re_τ with

blowing is observed for LES as well [3]. Nevertheless, the ODT flow properties are generally in good agreement with the reference LES data [3].

Table 2 The simulations results for friction Reynolds number Re_τ, displacement Reynolds number $Re_{\delta_{99}}$, momentum thickness Reynolds number Re_θ (f for final value of the quantities), skin friction C_f, von Kármán's constant K and shape factor H.

Case	$Re_{\tau,f}$	$Re_{\delta_{99},f}$	$Re_{\theta,f}$	$Re_{X,f}$ $[10^6]$	C_f $[10^{-3}]$	K	H
U1C1	848	3435	2479	1.2	4.04	0.28	1.38
U1C2	900	3646	2680	1.2	4.52	0.33	1.36
U1Z1	890	3604	2626	1.2	4.51	0.30	1.37
U1Z2	860	3483	2450	1.2	4.22	0.30	1.37
U1L1	933	3779	2818	1.2	5.11	0.34	1.34
U1L2	929	3764	2818	1.2	5.08	0.35	1.34
U1	876	3548	2583	1.2	4.30	0.32	1.37

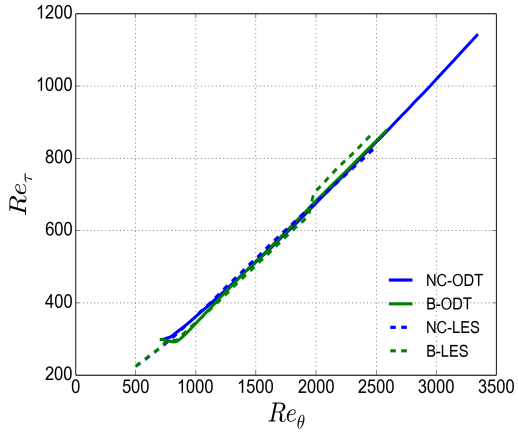

Fig. 10 The quantity Re_τ as a function of Re_θ up to $Re_\theta \approx 3000$ for uniform blowing (represented as 'B-') and non-blowing (represented as 'NC-' meaning 'no control') configurations. For comparison, the reference LES data from [3] is shown for corresponding configurations.

The shape factor, calculated as the ratio of the displacement thickness to the momentum thickness, $H = \delta/\theta$, over Re_θ is shown in Figure 11 along with the LES data from [3] as dashed lines for uniform blowing and non-blowing configurations. The shape factor allows a direct quantitative estimation of the mean streamwise velocity profile independent of the skin friction. Although the ODT profiles does not show good agreement with the LES data, we note an increase in H by blowing, which is similar to the reference data. In that sense, ODT captures the flow dynamics for the blowing configuration. This

indicates that the blowing can promote flow separation [3]. The shape factor is under-predicted by ODT as compared to the reference data. In the small Re_θ range a different H trend is observed for the ODT model. However, this trend is consistent with our earlier work [41,44]. At low Re_θ, the DNS trend is also different than the LES trend and a common trend line is reached at around $Re_\theta = 1000$ [15]. The values achieved for H for the cases considered for the present study are given in Table 2.

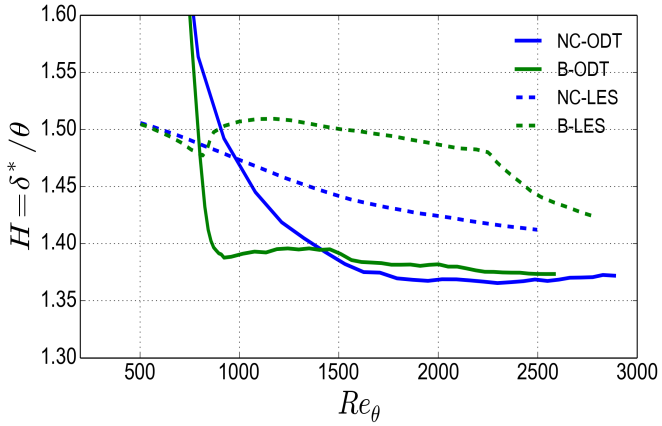

Fig. 11 The quantity H as a function of Re_θ up to $Re_\theta \approx 3000$ for uniform blowing (represented as 'B-') and non-blowing (represented as 'NC-' meaning 'no control') configurations. For comparison, the reference LES data from [3] is shown for corresponding configurations.

Finally, we show the development of the skin friction coefficient, $C_f = 2/(U_b^+)^2$, with Re_θ for cases with and without blowing using the ODT model along with the reference LES data from [3] for fixed free-stream velocity in Figure 12. C_f is calculated as the ratio of the wall shear stress to the dynamic pressure. Like the shape factor, the ODT skin friction coefficient also shows different trends in comparison to the LES data initially but the trend is consistent with the ODT literature [41,44]. The laminar-turbulent transition is induced at different Re_θ in the case of DNS [18]. DNS exhibit typical overshoots of C_f depending on the tripping of the turbulent transition and as a result, different behaviour of the simulations is reported in the region $Re_\theta = 200 - 1000$. The profiles are slightly over-predicted using the ODT methodology as compared to the reference data for the selected physical model parameters. However, it was under-predicted in [41,44]. The peak height can be altered by modifying the model parameters, nevertheless, the qualitative trends are sufficiently well reproduced with the chosen set of the model parameters.

Figure 12 also confirms the increase in the boundary layer thickness and decrease in the skin friction for uniform blowing configuration similar to the reference LES data reported in [3]. We achieve $\sim 15\%$ drag reduction in case

of blowing, in spite of the weak amplitude of the control, using a reduced order model. This confirms once again the overall consistency and the capability of the ODT model to predict such properties.

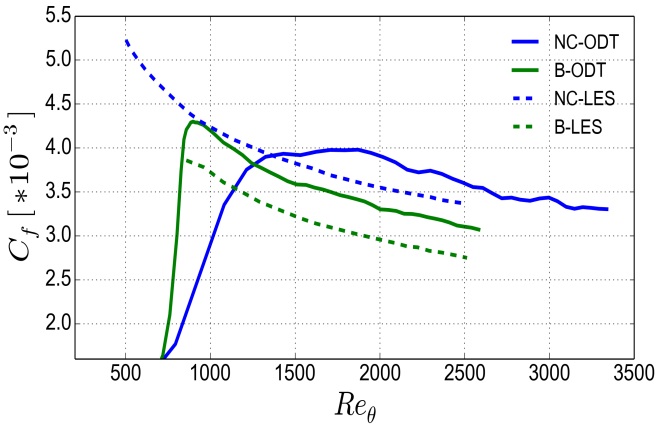

Fig. 12 The skin friction coefficient C_f as a function of Re_θ up to $Re_\theta \approx 3000$ for uniform blowing (represented as 'B-') and non-blowing (represented as 'NC-' meaning 'no control') configurations. For comparison, the reference LES data from [3] is shown for corresponding configurations.

6 Conclusion

In this paper, we investigated the effect of uniform blowing in a spatially developing turbulent boundary layer using a reduced order formulation, referred as ODT. The ODT model has been applied earlier to SBL and TBL type-flows without wall transpiration and also to a suction boundary layer, however, this is the first attempt to analyse the blowing boundary-layer-type flow and is another application of the model. We compared ODT results to the available reference LES data at various momentum thickness Reynolds numbers.

The computation of turbulent flows with blowing is of significant importance. Blowing leads to skin friction drag reduction, which has large economical and ecological impact from a fuel consumption viewpoint. Very high spatial resolution is required to resolve the full range of scales, and to gather complete information of the flow, especially in case of DNS. Hence, DNS and LES are limited to small and moderate momentum Reynolds numbers. However, in engineering applications, the Reynolds number is too high for practical computations.

A reduced order model is particularly appropriate for high Reynolds numbers. Due to the reduction in dimensionality in ODT, the flow variables are

resolved on a full range of time and length scales and the model is computationally efficient. The flow variables are evolved in two processes. First, the molecular diffusion is represented by a deterministic process. Second, the effects of turbulent advection and pressure fluctuation are modelled by a stochastic process.

We are aware from earlier studies that the ODT results are sensitive to the choice of the model parameters. Therefore, we conducted a parametric study to validate the uniform blowing formulation. While varying one parameter, others parameters were kept fixed and this was done for one Re_θ, i.e., at $Re_\theta \approx 2082$ in comparison with the LES data from [3] at same Re_θ. The model parameter α is consistent with the previous use of the ODT model and we have used $\alpha = 2/3$. The variation of C, Z and the LS method suggest a best fit for the mean velocity profile for $C = 6$, $Z = 100$ and the two-thirds suppression method. The optimal set of parameters provide sufficient confidence that the fundamental dynamics of the boundary layer flow are captured.

The calibrated model parameters were used for further simulations. We compared the velocity statistics, such as the mean, root mean square, and turbulent stresses as wall-normal profiles from our results with the LES [3] at various streamwise locations. We have also provided velocity statistics up to 4^{th} order for a uniform blowing configuration, however, we do not have corresponding LES data for comparison. The investigation was then extended to various global properties, for instance, the skin friction coefficient and shape factor. We report the key findings for the uniform blowing configuration as follows:

1. The mean streamwise velocity profile shows good agreement to the reference LES data for the spatially developing turbulent boundary layer with uniform blowing, indicating that the model is able to capture flow dynamics ranging from the viscous sublayer to the buffer layer into the logarithmic layer.
2. We confirm the well known artifact of the model and note that the peak amplitude of the rms velocity profile is under-predicted compared to the LES data which may be alleviated in the future by retaining 3-D information.
3. The Reynolds shear stress profiles show qualitative agreement with an overall under-prediction in comparison to the LES profiles. However, different trends are observed for various flow configurations [40,41,44] indicating that not all properties of a turbulent solution can be captured equally well under all circumstances.
4. The higher order velocity statistics are provided in comparison with the DNS of a non-blowing spatially developing turbulent boundary layer from [15] and the statistics are consistent with the previous applications of the model. However, we do not have these blowing statistics from DNS or LES.
5. The variation of all the velocity profiles with Re_θ is similar in comparison to the reference LES data for the blowing case considered.

6. We observed an increase in H with the blowing configuration, which is consistent with the reference LES data. However, overall, the shape factor profiles do not show good agreement with the reference data.
7. We achieve $\sim 15\%$ drag reduction in the blowing case using ODT, hence, confirming the overall consistency and the capability of the ODT model to predict such properties.

We close with noting that the comparison presented in this paper suggests that ODT is able to reproduce several LES velocity statistics for the spatially developing turbulent boundary layer with uniform blowing.

Acknowledgements R and HS acknowledge financial support from the Graduate Research School (GRS) of the BTU Cottbus-Senftenberg, Cluster StochMethod SP7, 'Stochastic Modeling of Turbulent Flow'.

Conflict of interest

The authors declare that they have no conflict of interest.

References

1. Y. Sumitani, N. Kasagi, AIAA Journal **33**, 1220 (1995)
2. Y. Kametani, K. Fukagata, Journal of Fluid Mechanics **681**, 154 (2011)
3. Y. Kametani, K. Fukagata, R. Örlü, P. Schlatter, International Journal of Heat and Fluid Flow **55**, 132 (2015)
4. K. Fukagata, S. Kern, P. Chatelain, P. Koumoutsakos, N. Kasagi, Journal of Turbulence **9**, N35 (2008)
5. S. Türk, G. Daschiel, A. Stroh, Y. Hasegawa, B. Frohnapfel, Journal of Fluid Mechanics **747**, 186– (2014)
6. H. Choi, P. Moin, J. Kim, Journal of Fluid Mechanics **262**, 75– (1994)
7. N. Kasagi, Y. Suzuki, K. Fukagata, Annual Review of Fluid Mechanics **41**, 231– (2009)
8. J. Kim, K. Kim, H. Sung, AIAA Journal **41**, 1697– (2003)
9. M. Pamiés, E. Garnier, A. Merlen, P. Sagaut, Physics of Fluids **19**, 108102 (2007)
10. V. Kornilov, A. Boiko, AIAA Journal **50**, 724– (2012)
11. K. Fukagata, K. Iwamoto, N. Kasagi, Physics of Fluids **14**, L73– (2002)
12. S. Yoshioka, J. Fransson, P.H. Alfredsson, Physics of Fluids **16**, 3530– (2004)
13. P.R. Spalart, Journal of Fluid Mechanics **187**, 61 (1988)
14. P. Schlatter, R. Örlü, Q. Li, G. Brethouwer, J.H.M. Fransson, A.V. Johansson, P.H. Alfredsson, D.S. Henningson, Physics of Fluid **21**, 051702 (2009)
15. P. Schlatter, R. Örlü, Journal of Fluid Mechanics **659**, 116 (2010)
16. J. Jiménez, S. Hoyas, M.P. Simens, Y. Mizuno, Journal of Fluid Mechanics **657**, 335 (2010)
17. T. Sayadi, C.W. Hamman, P. Moin, Journal of Fluid Mechanics **724**, 480 (2013)
18. P. Schlatter, R. Örlü, Journal of Fluid Mechanics **710**, 5 (2012)
19. I. Marusic, B.J. McKeon, P.A. Monkewitz, H.M. Nagib, A.J. Smits, K.R. Sreenivasan, Physics of Fluid **22**, 065103 (2010)
20. J. Wallace, Journal of Turbulence **13**, N53 (2012)
21. G. Eitel-Amor, R. Örlü, P. Schlatter, International Journal of Heat and Fluid Flow **47**, 57– (2014). DOI 10.1016/j.ijheatfluidflow.2014.02.006
22. A. Kerstein, Journal of Fluid Mechanics **392**, 277 (1999)
23. A. Kerstein, W. Ashurst, S. Wunsch, V. Nilsen, Journal of Fluid Mechanics **447**, 85 (2001)

24. R. Schmidt, A.R. Kerstein, S. Wunsch, V. Nilsen, Journal of Computational Physics **186**, 317 (2003)
25. R. Schmidt, A. Kerstein, R. McDermott, Computer Methods in Applied Mechanics and Engineering **199**, 865 (2010)
26. C. Glawe, J.A.M. M., H. Schmidt, Zeitschrift für Angewandte Mathematik und Mechanik **98**, 1907 (2018). DOI 10.1002/zamm.201800098
27. F. Schulz, C. Glawe, H. Schmidt, A. Kerstein, Environmental Earth Science **70**, 3739 (2013)
28. D.O. Lignell, A. Kerstein, G. Sun, E. Monson, Theoretical and Computational Fluid Dynamics **27**, 273 (2013)
29. D.O. Lignell, V.B. Lansinger, J. Medina, M. Klein, A.R. Kerstein, H. Schmidt, M. Fistler, M. Oevermann, Theoretical and Computational Fluid Dynamics **32**, 495 (2018)
30. J. Hewson, A. Kerstein, Combustion Theory and Modelling **5**, 669 (2001)
31. T. Echekki, A. Kerstein, T. Dreeben, Combustion and Flame **125**, 1083 (2001)
32. J. Hewson, A. Kerstein, Combustion Science and Technology **174**, 35 (2002)
33. E. Gonzales-Juez, A.R. Kerstein, D.O. Lignell, Journal of Fluid Mechanics **677**, 218 (2011)
34. D.O. Lignell, D.S. Rappleye, Combustion and Flame **159**, 2930 (2012)
35. H. Schmidt, A. Kerstein, R. Nédélec, S. Wunsch, B.J. Sayler, Theoretical and Computational Fluid Dynamics **27**, 377 (2013)
36. E.I. Monson, D.O. Lignell, M.A. Finney, C. Werner, Z. Jozefik, A.R. Kerstein, R.S. Hintze, Fire Technology **52**, 1 (2014)
37. Z. Jozefik, A. Kerstein, H. Schmidt, S. Lyra, H. Kolla, J. Chen, Combustion and Flame **162**, 2999 (2015)
38. E. Gonzales-Juez, R. Schmidt, A. Kerstein, Physics of Fluids **23** (2011)
39. A.R. Kerstein, S. Wunsch, Boundary Layer–Meteorology **118**, 325 (2006)
40. M.M. Fragner, H. Schmidt, Journal of Turbulence **18**, 899 (2017)
41. Rakhi, M. Klein, J.A.M. M., H. Schmidt, Journal of Turbulence **20**, 506 (2019). DOI 10.1080/14685248.2019.1674859
42. Rakhi, H. Schmidt, in *Proceedings of CMFF'18, 4-7 September 2018* (Budapest, Hungary, 2018)
43. Rakhi, H. Schmidt, Proceedings of Applied Mathematics and Mechanics **18**, e201800214 (2018). DOI 10.1002/pamm.201800214
44. Rakhi, H. Schmidt, in *Proceedings of TSFP-11, 30 July-2 August 2019* (Southampton, UK, 2019)
45. Rakhi, H. Schmidt, International Journal of Heat and Fluid Flow (2020 (Accepted))
46. J.C. Sutherland, N. Punati, A.R. Kerstein, A unified Approach to the Various Formulations of the One–Dimensional–Turbulence Model. Tech. Rep. ICSE100101, ICSE Report (2010)
47. W.T. Ashurst, A. Kerstein, Physics of Fluids **17** (2005)
48. S. Wunsch, A.R. Kerstein, Journal of Fluid Mechanics **528**, 173 (2005)
49. M. Kozul, D. Chung, J.P. Monty, Journal of Fluid Mechanics **796**, 437 (2016)